The chemical coupling between moist CO oxidation and gas-phase potassium sulfation

Chanpirak, Arphaphon; Hashemi, Hamid; Frandsen, Flemming J.; Wu, Hao; Glarborg, Peter; Marshall, Paul

Published in:
Fuel

Link to article, DOI:
10.1016/j.fuel.2022.127127

Publication date:
2023

Document Version
Publisher's PDF, also known as Version of record

Fuel 336 (2023) 127127

Contents lists available at ScienceDirect

Fuel

journal homepage: www.elsevier.com/locate/fuel

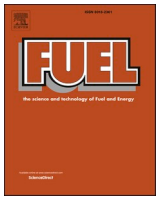

Full Length Article

The chemical coupling between moist CO oxidation and gas-phase potassium sulfation

Arphaphon Chanpirak [a], Hamid Hashemi [a], Flemming J. Frandsen [a], Hao Wu [a], Peter Glarborg [a,*], Paul Marshall [b]

[a] Department of Chemical and Biochemical Engineering, Technical University of Denmark, Søltofts Plads 229, 2800 Kgs. Lyngby, Denmark
[b] Department of Chemistry and Center for Advanced Scientific Computing and Modeling, University of North Texas, 1155 Union Circle #305070, Denton, TX 76203, USA

ARTICLE INFO

Keywords:
Potassium chloride (KCl)
Potassium hydroxide (KOH)
Sulfation
CO oxidation

ABSTRACT

In the present work, the chemical coupling between moist CO oxidation and transformation of gaseous potassium salts (KCl or KOH) in the presence and absence of SO_2 was investigated experimentally and through chemical kinetic modeling. The experiments were performed in a laminar flow quartz reactor at temperatures ranging from 873 to 1473 K. The experimental results showed that both KCl and KOH inhibited CO oxidation, but addition of SO_2 reduced the inhibiting effect by sulfating the potassium. The degree of sulfation of KCl and KOH by SO_2 was evaluated by EDX analysis of the aerosols collected downstream in a filter. Also, the consumption of SO_2 and, for KCl, the formation of HCl were indications of the level of sulfation. The results indicated that KCl was only sulfated to a small degree, consistent with the observation that addition of SO_2 had little effect on the inhibition of CO oxidation by KCl. Contrary to this, the captured KOH particles were fully sulfated according to the EDX results; however, most of the KOH was captured on the quartz reactor surface, forming potassium silicates.

The experimental results were interpreted in terms of a chemical kinetic model. Thermodynamic data for key potassium intermediates were re-evaluated by ab initio methods and the mechanism was updated according to recent results. The modeling predictions were in qualitative agreement with the experimental results for the effect of K/Cl/S on moist CO oxidation, but the degree of sulfation was strongly overpredicted for KCl. Analysis of the calculations indicates that sulfation pathways in the model involving $KOSO_3$ contribute to the overprediction, but both the thermodynamic properties and rate constants in the model involve significant uncertainties and more work is required to resolve the discrepancy.

1. Introduction

Waste-to-energy (WtE) plants and biomass-fired plants play an important role in the efforts to achieve a carbon–neutral society. It is important to achieve a high thermal efficiency and low emissions of harmful species from these units. The challenges, which include emission of pollutants (CO, NO_x, SO_x, dioxins) and particulate matter (PM), deposition (fouling and slagging), and corrosion of boiler surfaces, are in varying degree all linked to the inorganic elements in the fuel.

Biomass and waste fuels release inorganic elements (mainly K, Cl, and S) to the gas phase during thermal processes. The fraction of released inorganic content depends mostly on the type of fuel and the operational conditions [1]. Biomass may contain significant amounts of K, Cl, and Si; agricultural residues more so than woody biomass [2–6]. In municipal solid waste, the Cl content varies strongly depending on the source [7–11]. Alkali species released during devolatilization and/or char oxidation in the form of KCl, KOH, and K_2SO_4 [12] can be found in the gas phase and in aerosols. Gaseous KOH, rather than KCl and K_2SO_4, is detected at high temperatures in combustion of biomass high in K content and low in Cl and S [13,14]. In wood combustion, the level of KOH in the flue gas is typically higher than that of KCl [15]. As the flue gas is cooled in the superheater section, the alkali salts condense forming aerosols and sticky deposits. In the deposits, they may react with metal oxides and destroy the super-heater tubes [16,17]. In particular presence of KCl is associated with increased deposit formation [18] and accelerated corrosion [19].

* Corresponding author.
E-mail address: pgl@kt.dtu.dk (P. Glarborg).

https://doi.org/10.1016/j.fuel.2022.127127
Received 11 October 2022; Received in revised form 1 December 2022; Accepted 8 December 2022
Available online 15 December 2022

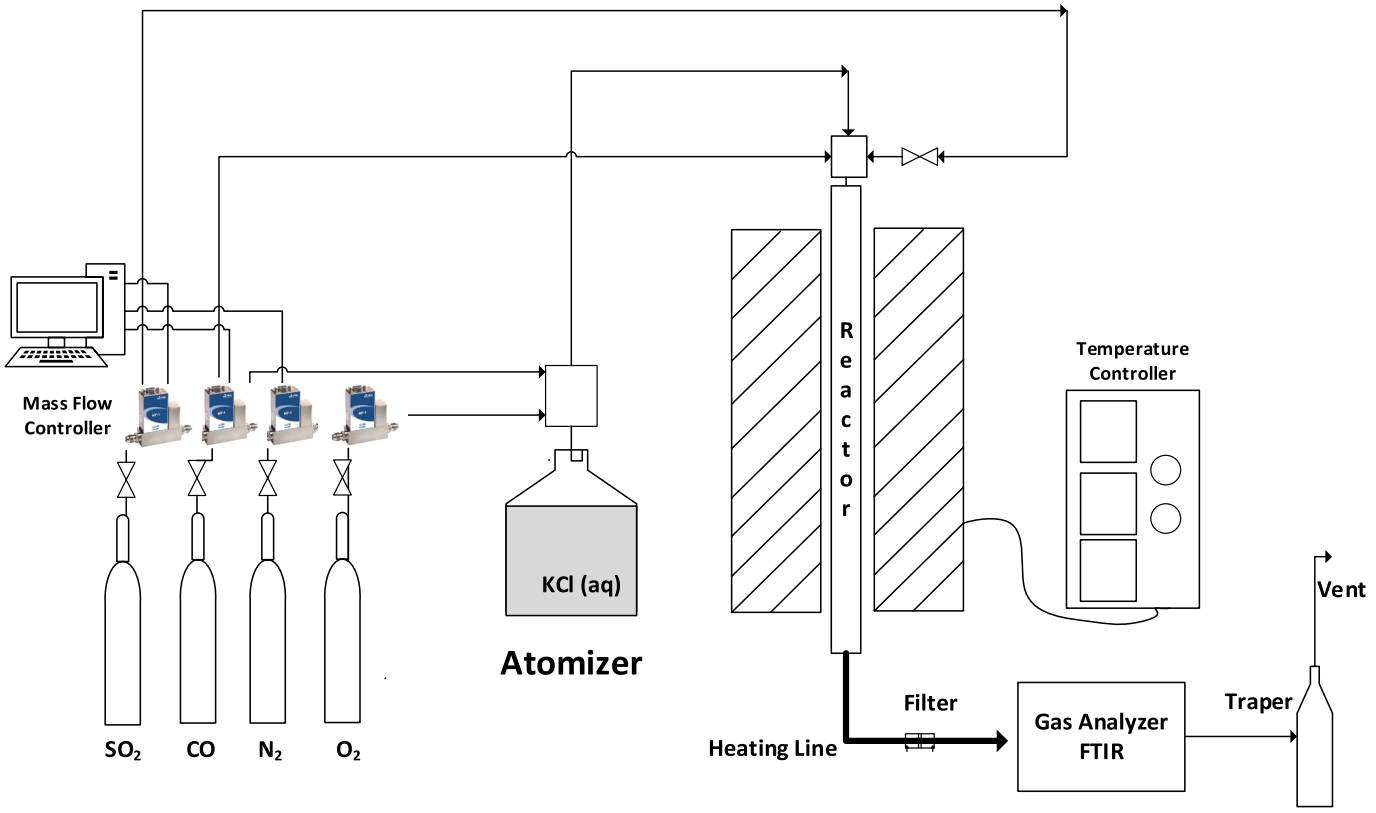

Fig. 1. Schematic of the flow reactor setup.

The emission of CO is strictly regulated, but often difficult to control in units burning waste and biomass due to the complexities of the fuel. The key reaction in CO oxidation is $CO + OH \rightleftarrows CO_2 + H$ (R1), which is controlled predominantly by the free radical pool in the gas phase. It has been shown that the rate of CO oxidation depends both on the composition of the flue gas and the presence of inorganic elements [20–22], but details of the chemical coupling between CO oxidation and alkali, chlorine, and sulphur species remain in question. Alkali species may act to recombine OH, H, O, and HO_2 radicals through gas-phase reactions at high temperature and result in inhibition or promotion of CO oxidation [20,23]. Previous studies [24] have suggested that this interaction involves the reactions $KCl + H \rightleftarrows K + HCl$ (R10b), $K + OH + M \rightleftarrows KOH + M$ (R6), $K + O_2 + M \rightleftarrows KO_2 + M$ (R7), $KO_2 + OH \rightleftarrows KOH + O_2$ (R8), and $KO + CO \rightleftarrows K + CO_2$ (R9) (the reaction numbers refer to Table 2 below).

Sulfur species are typically present in solid fuel combustion, released from the fuel-bound sulfur during combustion and/or added as sulfur powder, SO_2, or H_2SO_4 with the purpose of sulfating KCl [23,25–29]. Previous research has shown that SO_2 may inhibit or promote fuel oxidation, depending on conditions [20,21,30]. Tests in a 12-MW circulating fluidized bed (CFB) boiler has revealed that addition of elemental sulfur acts to reduce the inhibiting effect of potassium salts on CO oxidation during biomass combustion in a bed of olivine [25,27]. Berdugo Vilches et al. [28] carried out experiments in a post-flame environment in the temperature range 1100–1550 K and excess air ratios of 1.05–1.65 to investigate the influence of alkali and SO_2. They found that the inhibiting effect of potassium on the CO and H_2 oxidation, caused by chain-terminating reactions such as $K + OH + M \rightleftarrows KOH + M$ (R6) and $KO_2 + OH \rightleftarrows KOH + O_2$ (R8), was reduced in the presence of sulfur due to sulfation of the potassium. However, Ekvall and Andersson [29], who carried out an experimental and modeling study of C_3H_8 flames in a 100 kW test unit, found that KCl promoted the CO conversion with SO_2 addition under oxy-fuel conditions, while it had little effect when combusting in air. In a similar setup, Allgurén and Andersson [31] showed that KCl and SO_2 decreased the NO emission in both fuel-rich and oxygen-rich cases; this was attributed to enhanced consumption of OH radicals. Ekvall et al. [32] observed that the sulfation degree of the KCl with SO_2 increased in oxy-fuel conditions compared to air combustion.

Weng and co-workers [33,34] proposed a detailed chemical kinetic model for gas-phase sulfation of both KCl and KOH in the presence of SO_2 and compared predictions with results from co-flow and counter-flow laminar flames, measuring K, KOH, and KCl. Berdugo Vilches et al. [28] revised this model to describe the synergetic effects of K, S, and Cl-species related chemistry on CO oxidation. However, details of the mechanism are still open to discussion.

The current work investigates the influence of gaseous potassium salts (KCl or KOH) with and without SO_2 on CO oxidation in a flow reactor under fuel-lean conditions. The experimental work was carried out in a flow reactor with well-controlled feeding and accurate measurements of gases in a wide temperature range (873–1473 K). The degree of KCl/KOH sulfation by SO_2 was analyzed with SEM-EDX. The gas-phase experiments were combined with simulations using an updated kinetic reaction mechanism. The modeling was used to establish a fundamental understanding of the chemical coupling between CO oxidation and the alkali, sulfur, and chloride chemistry. The detailed chemical kinetic mechanism relies on previous work by the researchers [28,35,36], but is updated in the present work based on ab initio calculations for key alkali intermediates.

2. Experimental setup and procedure

A flow reactor setup as shown in Fig. 1 was developed for studying gaseous reactions. The setup consisted of a gas dosing system, an electrically heated flow reactor, a filter, a gas-product analysis unit, a gas manometer, and a cooling trap. A total gas flow rate of 2 NL/min (298 K, 1 atm), with an inlet CO concentration of 0.1 %, was used in all experiments. All gases with high purity of 99.995 % or higher were supplied from gas cylinders through a particulate filter and a series of

Table 1
Thermodynamic properties calculated in the present work for selected potassium species. Units are kcal or cal, mol, K.

Species	$H_{f,298}$	S_{298}	$C_{p,300}$	$C_{p,400}$	$C_{p,500}$	$C_{p,600}$	$C_{p,800}$	$C_{p,1000}$	$C_{p,1500}$
$KHSO_3$	−164.69	81.91	21.56	23.85	25.45	26.55	27.87	28.69	29.93
$KOSO_3$	−172.10	82.19	22.30	24.93	26.77	28.02	29.45	30.20	31.08
KSO_3Cl	−189.73	86.25	23.30	25.37	26.92	28.07	29.47	30.17	31.01

Table 2
Reactions most important for the chemical coupling between the moist CO oxidation and the alkali chemistry. The rate constants are in the form of $k \rightleftarrows AT^n \exp(-E/(RT))$. Units are mol, s, cm, cal, and K.

No.	Reactions	A	n	E	Note/ Reference
1	$H + O_2 \rightleftarrows O + OH$	1.0E14	0	15,286	[24]
2	$H + O_2(+M) \rightleftarrows HO_2(+M)$	4.7E12	0.44	0	[24]
	Low pressure limit	6.4E20	−1.72	5.25E02	
3	$CO + OH \rightleftarrows CO_2 + H$	8.7E05	1.73	−685	[24]
4	$SO_2 + O(+M) \rightleftarrows SO_3(+M)$	3.7E11	0	1689	[45]
	Low pressure limit	2.9E27	−3.58	5206	
5	$SO_3 + H \rightleftarrows SO_2 + OH$	8.4E09	1.22	3320	[45]
6	$K + OH + M \rightleftarrows KOH + M$	4.7E21	−1.26	0	est Na + OH + M
7	$K + O_2 + M \rightleftarrows KO_2 + M$	3.3E21	−1.55	19	[24]
8	$KO_2 + OH \rightleftarrows KOH + O_2$	2.5E15	−0.163	0	[24]
9	$KO + CO \rightleftarrows K + CO_2$	5.4E13	0	0	est NaO + CO
10	$K + HCl \rightleftarrows KCl + H$	9.1E12	0	1180	[41]
		1.0E14	0	3635	
11	$KO_2 + HCl \rightleftarrows KCl + HO_2$	1.4E14	0	0	est NaO_2 + HCl
12	$KOH + HCl \rightleftarrows KCl + H_2O$	1.7E14	0	0	est NaOH + HCl
13	$K + SO_2(+M) \rightleftarrows KOSO(+M)$	3.7E14	0	0	[41]
	Low pressure limit	5.2E23	−1.5	0	
14	$K + SO_3(+M) \rightleftarrows KOSO_2(+M)$	3.7E14	0	0	[41]
	Low pressure limit	4.7E34	−4.9	0	
15	$KO + SO_2(+M) \rightleftarrows KOSO_2(+M)$	3.7E14	0	0	[41]
	Low pressure limit	5.2E23	−1.5	0	
16	$KO_2 + SO_2(+M) \rightleftarrows KOSO_3(+M)$	1.0E14	0	0	[42]
	Low pressure limit	2.6E42	−7.6	0	
17	$KOH + SO_3(+M) \rightleftarrows KHSO_4(+M)$	1.0E14	0	0	[41]
	Low pressure limit	2.6E42	−7.6	0	
18	$KOSO_2 + O \rightleftarrows KO + SO_3$	1.3E13	0	0	[41]
19	$KOSO_2 + OH(+M) \rightleftarrows KHSO_4(+M)$	2.0E13	0	0	[42]
	Low pressure limit	1.0E23	−1.5	0	
20	$KOSO_2 + KO \rightleftarrows K_2SO_4$	1.0E14	0	0	[41]
21	$KOSO_3 + O \rightleftarrows KOSO_2 + O_2$	1.0E14	0	0	[42]
22	$KOSO_3 + KOH \rightleftarrows K_2SO_4 + OH$	1.0E14	0	0	[42]
23	$KHSO_4 + H \rightleftarrows KOSO_2 + H_2O$	2.0E13	0	0	[42]
24	$KHSO_4 + OH \rightleftarrows KOSO_3 + H_2O$	1.0E12	0	0	est $HOSO_2$ + OH
25	$KHSO_4 + KOH \rightleftarrows K_2SO_4 + H_2O$	1.0E14	0	0	[41]
26	$KCl + SO_3(+M) \rightleftarrows KSO_3Cl(+M)$	1.0E14	0	0	[41]
	Low pressure limit	1.9E41	−7.8	0	
27	$KSO_3Cl + H_2O \rightleftarrows KHSO_4 + HCl$	1.0E14	0	0	[41]
28	$KHSO_4 + KCl \rightleftarrows K_2SO_4 + HCl$	3.0E13	0	0	Pw
29	$KSO_3Cl + K \rightleftarrows KOSO_2 + KCl$	2.0E13	0	0	[42]
30	$KSO_3Cl + KOH \rightleftarrows K_2SO_4 + HCl$	1.0E14	0	0	[41]

precise mass flow controllers (EL-FLOW® Thermal Mass Flow Controllers, model series: F-201CV, made by Bronkhorst High-Tech B.V.).

The dosing system for submicrometer-sized KCl/KOH droplets employed a constant output atomizer (Model 3076, TSI Inc. Particle Instruments, St. Paul, USA), which had been utilized in other studies [37–39]. The atomizer generated aerosols with a mean particle size in a range of 0.02–0.3 μm [40]. The total volume of solution in the plastic-coated glass bottle was 1000 mL. The solution was prepared by using KCl or KOH powder (≥99.9 %, Sigma-Aldrich Corp.) and deionized water. The carrier gas passed through an orifice of the atomizer body. The gas and the generated droplets were introduced into the reactor through a tube. The inner diameter of the tube was 12 mm with the same size as the atomizer outlet, and the tube was designed to minimize the impact of condensation. To verify a stable and continued flow of droplets from the atomizer, the water vapor concentration was measured by an FTIR (MKS MultiGasTM 2030) at an operating temperature of 453 K. The results, shown as Supplementary Data, confirm that the feeding of aerosols was stable.

The gaseous reactant and aerosol flows were mixed in a vessel above the main reactor. The main reactor was made of quartz with an inner diameter of 6 mm and a height of 900 mm. The reactor tube was placed in a temperature-controlled electrically heated oven. The axial temperature profile in the reactor in a nitrogen atmosphere was measured by insertion of a type K thermocouple from the top. As can be seen from the measured temperature profile in Supplementary Data, the length of the isothermal section was approximately 400 mm. The uncertainty in the isothermal temperature, ±10 K, includes the measurement accuracy (±2 K) and the deviation from the mean value. A quartz filter was installed downstream of the main reactor to collect fine particles. The product gas line and a filter were maintained at 453 K by a heating element cable to avoid the condensation of water and sulfur-containing compounds. Experiments were performed at a temperature range of 873–1473 K and at atmospheric pressure.

The concentrations of CO, CO_2, SO_2, H_2O, and HCl in the gaseous product stream were continuously monitored by a Fourier Transform Infrared spectrometer (FTIR) (Multigas 2030 FTIR, MKS instruments) at 453 K. The uncertainty in the gas analyzer measurements was below 10 %. The elemental composition and the morphology of the collected particles were characterized using scanning electron microscopy coupled with energy-dispersive X-ray spectroscopy (SEM-EDX) (Prisma E-SEM, Thermo Fisher Scientific). To reduce the uncertainty, the EDX measurements were performed at five areas in each sample, based on a similar color area of images and repeatable measurements. For imaging and EDX analysis, an accelerating voltage of 20 kV was employed.

3. Detailed chemical kinetic model

The reaction mechanism and thermodynamic data were based on previous work on alkali chemistry by Glarborg and Marshal [41], Hindiyarti et al. [42], Li et al. [43], Weng et al. [35], Berdugo Vilchez et al. [28], and Chanpirak et al. [24], together with subsets for chlorine [44], sulfur [45], and moist CO oxidation [24]. Table 1 shows thermodynamic properties for species revised in the present work, while Table 2 lists reactions important for the chemical coupling between the moist CO oxidation and the alkali chemistry.

Glarborg and Marshall [41] proposed a detailed reaction mechanism for the formation of K_2SO_4 in the gas phase, claiming the oxidation of SO_2 to SO_3 to be the rate-limiting step. This reaction mechanism, which

Table 3
Experimental conditions for the CO oxidation with/without KOH/KCl and SO_2.

Set	Inlet gases				Additive (aerosol)		
	CO (ppm)	O_2 (vol %)	SO_2 (ppm)	NO (ppm)	H_2O (vol%)	KCl (ppm)	KOH (ppm)
1	–	5.0	750	–	3.2	–	–
2	1000	5.0	–	–	3.2	–	–
3	1000	5.0	750	–	3.2	–	–
4	1000	5.0	–	–	3.2	212	–
5	1000	5.0	–	–	3.2		212
6	1000	5.0	750	–	3.2	212	–
7	1000	5.0	750	–	3.2	–	212
8	1000	5.0	300	–	3.2	–	212
9	1000	0.75	–	–	3.2	–	–
10	1000	0.75	750	–	3.2	–	–
11	1000	0.75	–	–	3.2	212	–
12	1000	0.75	–	–	3.2	–	212
13	1000	0.75	750	–	3.2	212	–
14	1000	0.75	750	–	3.2	–	212
15	1000	0.75	0	200	3.2	–	212
16	1000	0.75	750	200	3.2	–	212

was shown to be consistent with the entrained flow reactor results of Iisa et al. [46] on sulfation of KCl, involved the following reaction sequence: $KCl + SO_3 (+M) \rightleftarrows KSO_3Cl (+M)$ (R26), $KOH + SO_3 (+M) \rightleftarrows KHSO_4 (+M)$ (R17), $KSO_3Cl + H_2O \rightleftarrows KHSO_4 + HCl$ (R27), $KHSO_4 + KCl \rightleftarrows K_2SO_4 + HCl$ (R28), $KHSO_4 + KOH \rightleftarrows K_2SO_4 + H_2O$ (R25). Glarborg and Marshall emphasized the importance of alkali hydrogen sulfates as gas-phase precursors of A_2SO_4, and estimated the thermodynamic properties of $KHSO_4$ and selected chlorinated intermediates from ab initio computations. Hindiyarti et al. [42] proposed a number of additional pathways to sulfation of KCl and KOH, involving $KHSO_3$ and $KOSO_3$, to improve the prediction of sulfation at lower temperature. More recently, additional modifications were made to the potassium subset [28,35,43]. The reaction mechanism represents homogeneous nucleation of gaseous K_2SO_4 as an irreversible first-order reaction of $K_2SO_4 \rightarrow K_2SO_4(c)$ with a rate constant of 1E-61 exp(300000/*T*) s^{-1}, estimated based on aerosol theory [43].

In the present work, thermodynamic properties were updated for $KHSO_3$, $KOSO_3$ and KSO_3Cl using the methods described in ref. [41], with G3 theory replaced by G4 [47]. The revised thermodynamic properties are listed in Table 1. The updated values for the heat of formation of $KOSO_3$ is more than 5 kcal/mol lower than that calculated by Hindiyarti et al. [42], while for $KHSO_3$ and KSO_3Cl the present calculations agree within 1.5 kcal/mol with previous estimates [41,42].

In the reaction mechanism, a check was made to ensure that rate constants for reactions involving potassium species with updated thermodynamic properties were below the collision frequency in both the forward and reverse direction. This has implications for the reaction $KHSO_4 + KCl \rightleftarrows K_2SO_4 + HCl$ (R28) where the rate constant was lowered by a factor of 3 in the present work.

4. Results and discussion

Flow reactor experiments on the $CO/O_2/H_2O$ system strongly diluted in N_2 in the absence and presence of gaseous KCl/KOH and/or SO_2 were performed under fuel-lean conditions (1000 ppm CO and 0.75 % or 5 % O_2) and at atmospheric pressure. Table 3 lists the experimental conditions. The experimental data at each condition were obtained as the steady-state value.

The kinetic modeling in the present work was conducted in ANSYS Chemkin Pro using the plug flow reactor configuration for an isothermal reactor. At the inlet of the reactor, the water in the aerosol was assumed to evaporate instantaneously and the potassium to be distributed between condensed and gas-phase according to chemical equilibrium at the temperature of the isothermal zone. The calculated fraction of the K-salt in the gas phase is shown as Supplementary Data.

According to the experimental data obtained in the current work, discussed below, and consistent with results from literature, gaseous KOH reacts rapidly with the quartz surface of the flow reactor to form potassium silicates. This reaction is included in the model as a pseudo-first-order reaction for loss of KOH. Assuming it to be diffusion-limited, we estimate a rate constant of $10^{-4}\ T^{1.75}\ s^{-1}$. Also gaseous KCl reacts with the quartz reactor walls [28], but this step is slower and was not accounted for in the modeling.

4.1. Effect of KCl and SO_2 on moist CO oxidation

4.1.1. CO oxidation at reference conditions

Reference experiments on CO oxidation in the absence of both potassium and SO_2 were carried out with 0.75 % O_2 and 5 % O_2. The results are shown in Fig. 2. The CO oxidation can be characterized by the temperature T_i for initiation of reaction and the temperature T_{50} for 50 % conversion. For 0.75 % O_2, $T_i = 1020$ K and $T_{50} = 1050$ K, while at 5 % O_2, the corresponding values are $T_i \geq 1025$ K and $T_{50} = 1075$ K. The results show that under the present conditions CO conversion is inhibited with increasing O_2 concentration.

The modeling predictions, shown as solid lines in Fig. 2, are in

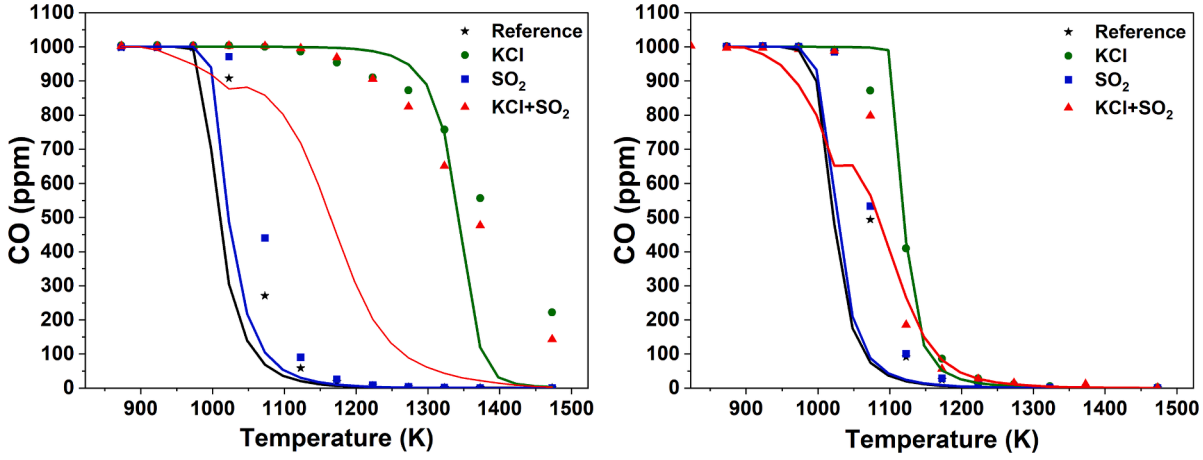

Fig. 2. The concentration of CO in the product gas as a function of temperature in a system containing $CO-O_2-H_2O$ with/without the KCl/SO_2 presence. Comparison between experimental data (symbols) and modeling predictions (lines) for CO. The reference condition includes only CO, O_2, and H_2O as reactants. Inlet condition: 1000 ppm CO, 0.75 % O_2 (left), 5 % O_2 (right), 3.2 % H_2O, 750 ppm SO_2, 212 ppm KCl, and N_2 balance. The residence time is 92/T(K) in the isothermal area at 823–1473 K.

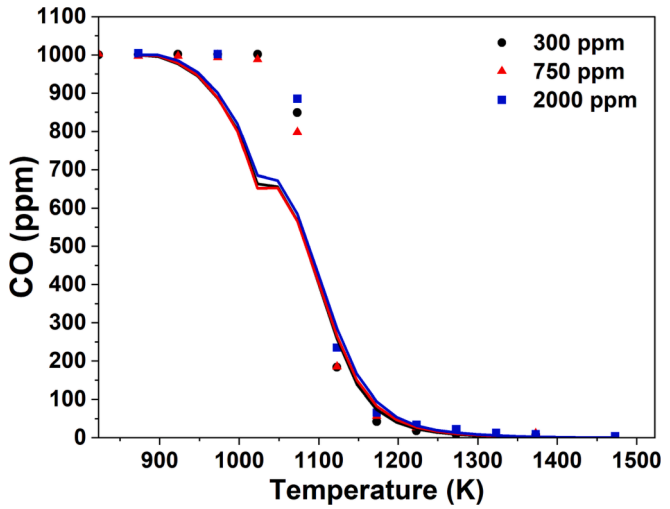

Fig. 3. Comparison of measured and predicted data for CO in the CO/KCl/SO_2/O_2/H_2O system. Inlet conditions: 1000 ppm CO, 212 ppm KCl, 300, 750, or 2000 ppm SO_2, 5 % O_2, 3.2 % H_2O; N_2 balance. The residence time is 92/T(K) in the isothermal area at 823–1473 K. Symbols denote experimental data; solid lines denote modeling prediction results.

satisfactory agreement with the experimental results, even if the model slightly under-predicts the onset temperature for CO oxidation. The effect of O_2 is captured well by the model. A sensitivity analysis for CO_2 formation is presented in the Supplementary Data. It shows that the $H + O_2 + M \rightleftarrows HO_2 + M$ reaction (R2) is a rate-limiting step for both oxygen levels, explaining why an increase in O_2 acts to slow down CO oxidation. Formation of HO_2, which is a comparatively unreactive radical, has an inhibiting impact on the CO conversion; in particular due to the competition with the chain-branching step $H + O_2 \rightleftarrows O + OH$ (R1).

4.1.2. *Effect of SO_2 on CO oxidation*

As seen in Fig. 2, the addition of SO_2 (without any potassium) results in a slight suppression of the CO oxidation compared with the reference condition. For 0.75 % O_2, the addition of SO_2 increases the initiation temperature of CO conversion (T_i) and T_{50} by around 20 K. For 5 % O_2, the effect of SO_2 is within the experimental uncertainty. The results are in good agreement with observations reported in the literature [21,30,48]. Similar to the reference conditions, the model under-predicts the onset of reaction for CO for both oxygen levels, but the small effect of SO_2 is captured well.

4.1.3. *Effect of KCl on CO oxidation*

As reported by Chanpirak et al. [24], KCl inhibits strongly the CO oxidation in a flow reactor at atmospheric pressure and 773–1373 K. This is confirmed by the results illustrated in Fig. 2. At 0.75 % O_2, addition of 212 ppm KCl shifts the T_i and T_{50} for CO consumption upward by around 150 K and 300 K, respectively, compared to the reference case. The model captures the experimental results fairly well, even though there is an under-prediction of CO above 1373 K.

At 5 % O_2, addition of 212 ppm KCl yields a value of T_i of approximately 1023 K; similar to the reference condition. The inhibition effect of KCl occurs in the temperature range of 1023–1223 K. The experimental and predicted results for the CO-KCl system are in reasonable agreement.

4.1.4. *Effect of SO_2 on CO oxidation in the presence of KCl*

The effect of adding SO_2 on CO conversion in an atmosphere with KCl is illustrated in Fig. 2. The inhibition of CO oxidation caused by KCl is slightly reduced by the addition of SO_2. The initiation temperature T_i in the CO/KCl system is similar at 1173 K with and without SO_2 addition at 0.75 % O_2 (Fig. 2 (a)), while 50 % conversion of CO was obtained at a slightly lower temperature in the presence of SO_2; still, the T_{50} of 1350–1375 K represents a shift of about 350 K compared to the reference condition. Also at 5 % O_2 (Fig. 2 (b)), the SO_2 addition slightly promotes the CO conversion rate in the presence of KCl, most pronounced in the 1023–1223 K range.

The model significantly overestimates the effect of SO_2 on the CO/KCl system for both oxygen levels, predicting a much larger promotion of oxidation for the CO/KCl system in the presence of SO_2 than observed experimentally. The difference between experiment and modeling is most pronounced at 0.75 % O_2, where there is a shift in the profile for CO of about 200 K. As discussed by Berdugo Vilches et al. [28], the inhibiting effect of potassium salts on CO oxidation is reduced in the presence of sulfur oxides due to the gas-phase sulfation of the potassium. The sulfation yields K_2SO_4, which contrary to KCl and KOH is believed not to be active in promoting radical recombination. The discrepancy in the modeling predictions is mainly attributed to over-prediction by the model of the degree of sulfation, as discussed further below.

Fig. 3 shows the effect of different SO_2 concentrations (300, 750, and 2000 ppm) on CO oxidation with 5 % O_2 and in the presence of KCl. Similar concentration profiles of CO are obtained for the three conditions; the differences are within experimental uncertainty. The independence of the moist CO oxidation with respect to the SO_2 concentration is also captured by the model. However, the predictions overestimate the oxidation rate below 1100 K.

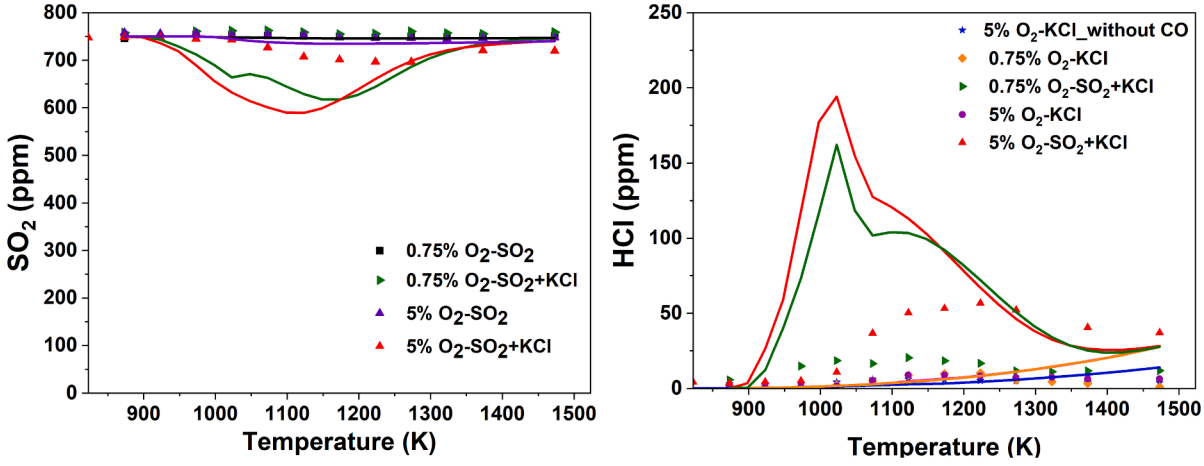

Fig. 4. Comparison of measured and predicted data for SO_2 (left) and HCl formation (right) in the product gas in the CO/KCl /SO_2/O_2/H_2O system. Inlet conditions: 0 or 1000 ppm CO, 0 or 212 ppm KCl, 750 ppm SO_2, 0.75 % or 5 % O_2, 3.2 % H_2O; N_2 balance. The residence time is 92/T(K) in the isothermal area at 823–1473 K. Symbols denote experimental data; solid lines denote modeling prediction results.

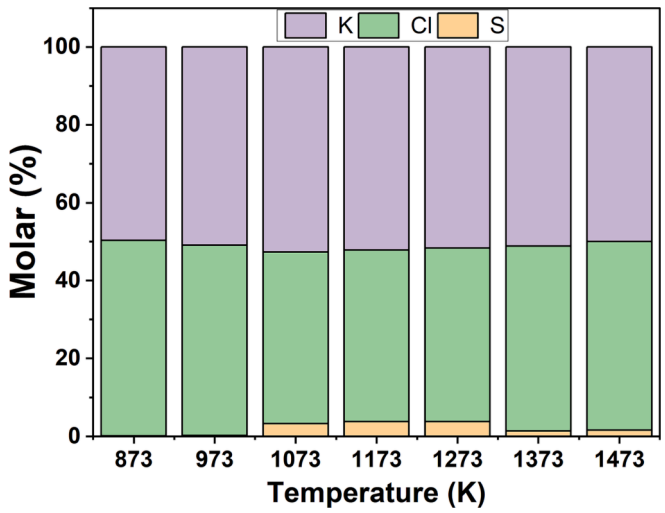

Fig. 5. SEM-EDX analysis of the collected samples for the KCl/SO_2/CO/O_2/H_2O system. Data for oxygen and carbon are excluded. Inlet condition: 1000 ppm CO, 212 ppm KCl, 750 ppm SO_2, 5 % O_2, 3.2 % H_2O; N_2 balance (corresponding to Fig. 2).

4.1.5. *Sulfation of KCl by SO_2*

The overall reaction for sulfation of KCl can be written as $2KCl + SO_2 + ½O_2 + H_2O \rightarrow K_2SO_4 + 2HCl$. The sulfation thus consumes SO_2 while it yields gaseous HCl, along with potassium sulfate aerosols that can be captured downstream in the filter. Both the SO_2 and HCl concentrations in the product gas and the content of S in the filter sample are measures of the degree of sulfation.

Fig. 4 compares experimental and numerical concentrations for outlet SO_2 and HCl for the investigated conditions. As indicated in Fig. 4 (upper), the SO_2 profile in the CO-SO_2-H_2O system is insensitive to temperature and oxygen concentration. In the presence of KCl, some SO_2 is consumed at the high oxygen concentration in the 1050–1350 K range; up to a maximum of 50 ppm at approximately 1000 K. For 0.75 % O_2 the SO_2 concentration remains unchanged. In the simulation, the SO_2 consumption in the presence of KCl is over-predicted under the investigated conditions, while the model predicts correctly that the SO_2 outlet is unchanged over the entire temperature in the SO_2/O_2/H_2O experiment.

Fig. 4 (lower) compares experimental and calculated data for HCl in the product gas. Hydrogen chloride is observed even in the absence of SO_2. For the KCl/H_2O/O_2 and CO/KCl/H_2O/O_2 systems, the HCl profiles are similar; CO has no effect on HCl formation. As proposed by Chanpirak et al. [24], the formation of HCl with no SO_2 addition can be explained by the heterogeneous KCl + SiO_2 reaction at the quartz reactor surface, forming potassium silicates.

In the presence of SO_2, the HCl yield is clearly enhanced; the difference can be attributed to KCl sulfation. The HCl formation is increased at higher O_2 levels; the maximum concentration of HCl is about 20 ppm at 0.75 % O_2 and 60 ppm at 5 % O_2. Results for varying SO_2 levels (corresponding to the conditions in Fig. 3) show the hydrogen chloride concentration to increase with the SO_2 level, supporting the role of sulfation in HCl formation (see Supplementary Data).

The simulation results significantly over-predicts the HCl formation at all the SO_2 levels (Fig. 4 and Supplementary Data). Also, the predicted peak of HCl is shifted to lower temperatures compared to experimental data. As discussed, the formation of HCl may be attributed to gas-phase reactions, i.e., $KCl + H_2O \rightleftarrows KOH + HCl$ (R12b) or sulfation ($2KCl + SO_2 + ½O_2 + H_2O \rightleftarrows K_2SO_4 + 2HCl$), or to the heterogeneous reaction of KCl with SiO_2 at the quartz reactor surface. According to the model, the conversion of KCl to KOH is very limited, and the discrepancy is primarily caused by over-prediction of the KCl sulfation.

SEM-EDX analyses were used to identify the chemical composition of the samples collected on the filter in the downstream line of the KCl-CO-SO_2 experiments. The results for 5 % O_2 for different temperatures are presented in Fig. 5, shown as the molar percentage of the major inorganic elements, i.e., K, Cl, and S. The elemental composition of the samples for 0.75 % O_2 is shown as Supplementary Data.

For both oxygen levels, the results reveal that the isothermal zone temperature affects the element composition in the particles captured downstream. The fine particles consist of K, S, and Cl in fractions consistent with a mixture of KCl and K_2SO_4. Sulfur is mainly detected in the samples obtained for reactor temperatures in the range 1073–1273 K. Here, the S content is around 4–5 %, showing that the fine particles are composed mainly of KCl with some K_2SO_4. The results indicate that the gaseous KCl is partly sulfated by reaction with SO_2 to form a K_2SO_4 aerosol. Sulfation of condensed KCl by a gas–solid reaction with SO_2 is very slow at low temperature [49] and reaction in the filter can be disregarded. Below 1000 K and above 1350 K, no or little sulfur is detected in the samples; the particles consist largely of KCl.

Fig. 6 compares the measured and predicted molar ratio of S/(Cl + S) in the filter deposits, as a measure of the degree of gas-phase sulfation in the reactor. For both levels of oxygen, the measured degree of sulfation

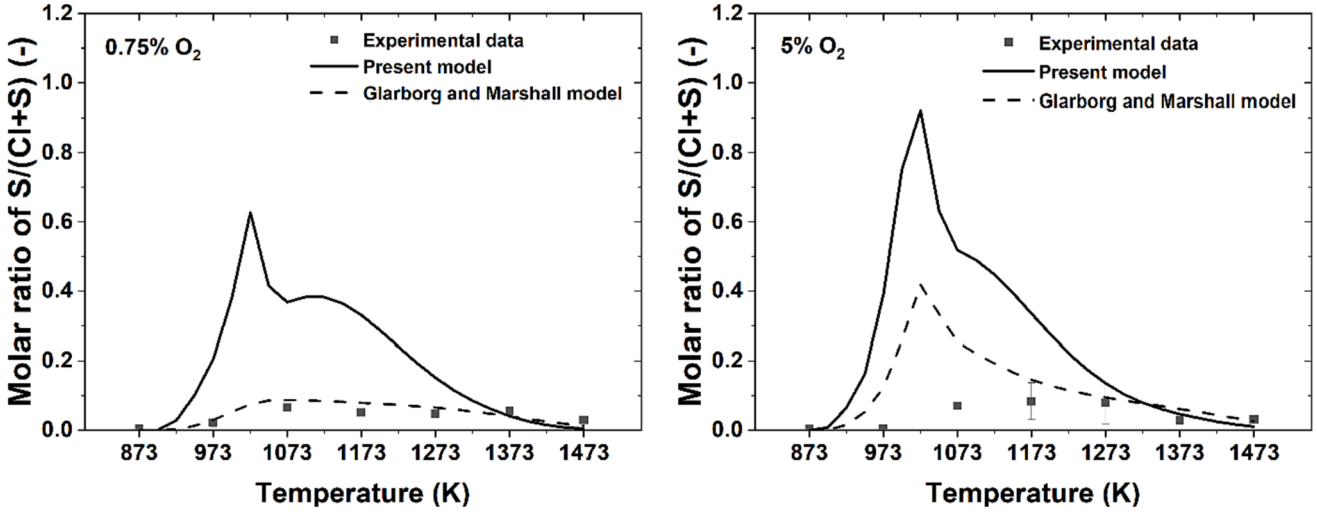

Fig. 6. Comparison of experimental and predicted molar ratios of S/(Cl + S) of the collected particle samples in the CO/KCl/SO_2/O_2/H_2O system with 0.75 % O_2 (left) and 5 % O_2 (right). Inlet condition: 1000 ppm CO, 212 ppm KCl, 750 ppm SO_2, 0.75 % or 5 % O_2, 3.2 % H_2O; N_2 balance (as in Fig. 2). Symbols denote experimental data; lines denote modeling predictions with the present model (solid) and the model of Glarborg and Marshall [41] (dashed).

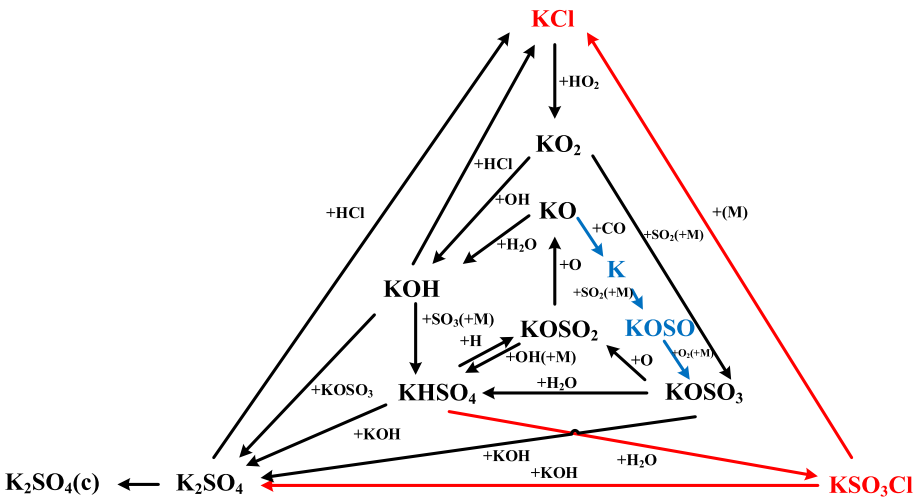

Fig. 7. Simplified reaction path diagram for transformation of KCl and KOH in moist CO oxidation (5% O_2) in the presence of SO_2. Black arrows denote pathways common for KCl and KOH, while the red and blue arrows denote paths specific for KCl and KOH, respectively. (For interpretation of the references to color in this figure legend, the reader is referred to the web version of this article.)

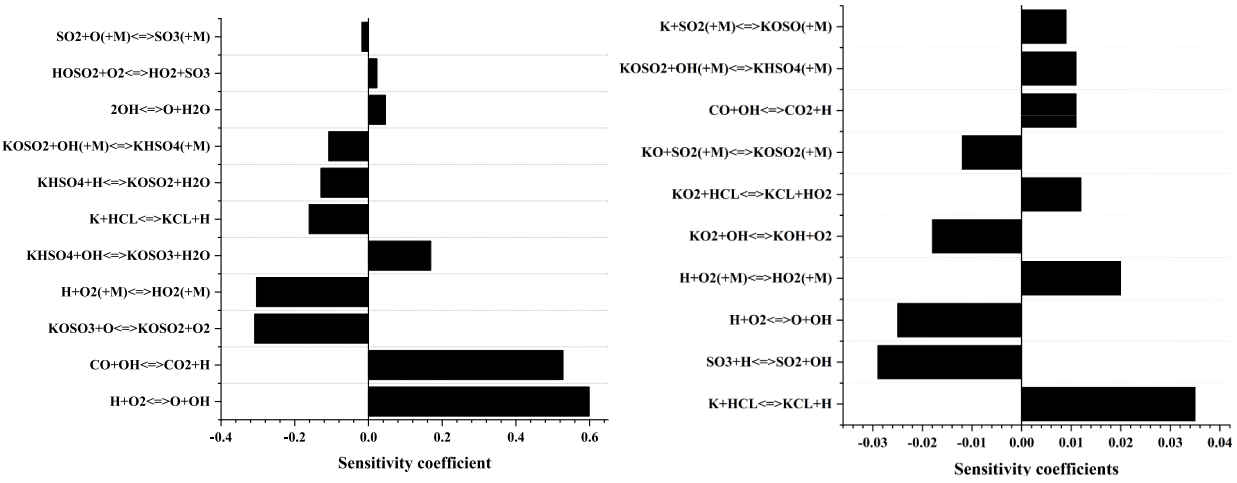

Fig. 8. A-factor sensitivity coefficients for prediction of CO_2 formation (left) at 50 % conversion (1080 K) and K_2SO_4 (right) (1173 K) for conditions corresponding to Fig. 2 (upper).

of KCl by SO_2 is quite low. However, a higher level of O_2 is seen to accelerate slightly the conversion of KCl into K_2SO_4 aerosols.

The results of Fig. 6 clearly confirms that the present model over-predicts the degree of sulfation in the CO/KCl/SO_2/O_2 system, in line with the discrepancies found for SO_2 and HCl in Fig. 4. The figure also shows predictions with the model of Glarborg and Marshall [41], which are in better agreement with experiment. To understand the possible reasons for the short-comings of the present model and the improved prediction of the Glarborg and Marshall mechanism, reaction path and sensitivity analyses for the predicted K_2SO_4 formation were conducted and they are discussed below.

4.1.6. Reaction path and sensitivity analyses

Fig. 7 shows the potassium species transformation according to the model for moist CO oxidation at 5 % O_2 in the presence of SO_2. The main path for sulfation of gaseous KCl involves the following sequence,

$$KCl + HO_2 \rightleftarrows KO_2 + HCl \quad (R2)$$

$$KO_2 + SO_2 + M \rightleftarrows KOSO_3 + M \quad (R16)$$

$$KOSO_3 + H_2O \rightleftarrows KHSO_4 + OH \quad (R24b)$$

$$KOSO_3 + KOH \rightleftarrows K_2SO_4 + OH \quad (R22)$$

$$KHSO_4 + KOH \rightleftarrows K_2SO_4 + H_2O \quad (R25)$$

The K_2SO_4 aerosol is then formed by homogeneous nucleation, represented in the model as an irreversible pseudo first-order reaction, $K_2SO_4 \rightarrow K_2SO_4(c)$.

Sensitivity analyses for the predicted concentrations of CO_2 and K_2SO_4 are shown in Fig. 8. The analysis indicates that the consumption and generation of free radicals in the system control the oxidation of CO (left figure). It is promoted by reactions that replenish the free radical pool, i.e., $CO + OH \rightleftarrows CO_2 + H$ (R1), $H + O_2 \rightleftarrows O + OH$ (R2), and $2OH \rightleftarrows O + H_2O$, and suppressed by the competing reaction $H + O_2 (+M) \rightleftarrows HO_2 (+M)$ (*R3*). Considering K-species reactions, $KOSO_3 + O \rightleftarrows KOSO_2 + O_2$ (R21), $KHSO_4 + OH \rightleftarrows KOSO_3 + H_2O$ (R24), $KHSO_4 + H \rightleftarrows KOSO_2 + H_2O$ (R23), and $KOSO_2 + OH + M \rightleftarrows KHSO_4 + M$ (R19) all serve to suppress CO oxidation as a result of consuming OH, H and O radicals, while $KCl + H \rightleftarrows K + HCl$ (R10b) promotes CO conversion. The chain-terminating step $SO_2 + O (+M) \rightleftarrows SO_3 (+M)$ (R4)) also inhibits the oxidation of CO.

The sensitivity coefficients for K_2SO_4 are fairly small, indicating that the rate constants in the model has only a limited impact on the predicted degree of sulfation. The reactions $CO + OH \rightleftarrows CO_2 + H$ (R1) and

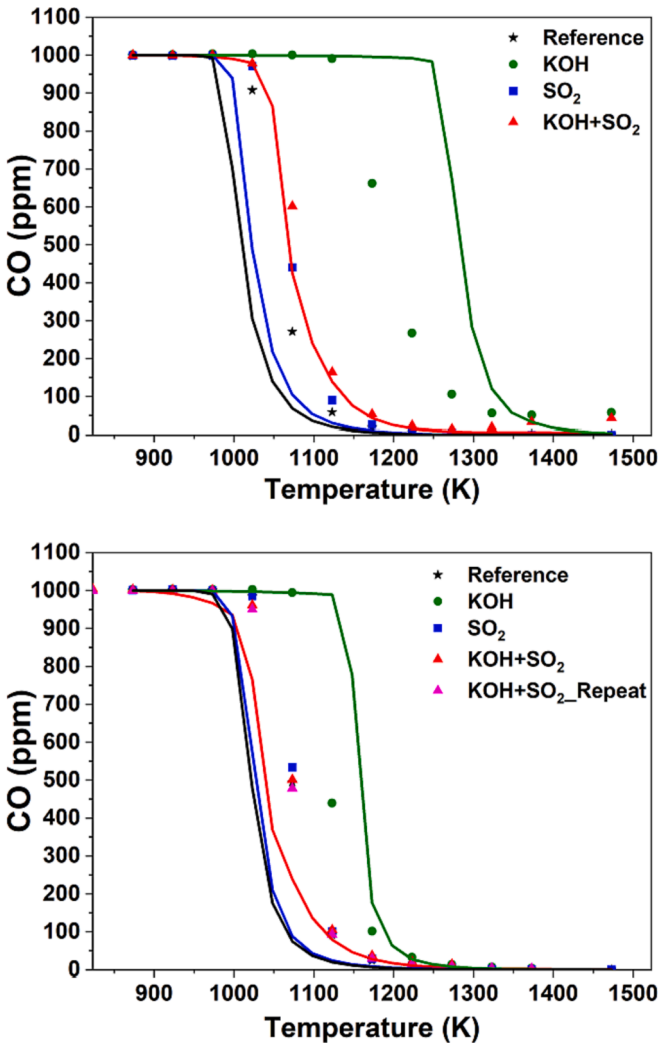

Fig. 9. The concentration of CO in the product gas as a function of temperature in a system containing CO-O_2-H_2O with/without KOH and/or SO_2. Comparison between experimental data (symbols) and modeling predictions (lines) for CO. The reference condition: CO-O_2-H_2O without the presence of KOH or SO_2. Inlet condition: 1000 ppm CO, 212 ppm KOH, 750 ppm SO_2, 0.75 % O_2 (a), 5 % O_2 (b), 3.2 % H_2O; N_2 balance. The residence time is 92/T(K) in the isothermal area at 823–1473 K.

$SO_2 + OH \rightleftarrows SO_3 + H$ (R5b) have positive sensitivity coefficients, confirming that oxidation of SO_2 to SO_3 formation is a significant step promoting sulfation of KCl. In the absence of CO, the degree of sulfation is significantly reduced, showing the importance of radicals in the sulfation of KCl. The composition of the O/H radical pool is important, with $H + O_2 (+M) \rightleftarrows HO_2 (+M)$ (*R*3) promoting sulfation, while $H + O_2 \rightleftarrows O + OH$ (R2) is inhibiting. Other reactions with a positive sensitivity include, $KCl + HO_2 \rightleftarrows KO_2 + HCl$ (R11b), $KOSO_2 + OH (+M) \rightleftarrows KHSO_4 (+M)$ (R49), and $K + SO_2 (+M) \rightleftarrows KOSO (+M)$ (R13). The reactions $KCl + H \rightleftarrows K + HCl$ (R10b), $KO + SO_2 (+M) \rightleftarrows KOSO_2 (+M)$ (R5), and $KO_2 + OH \rightleftarrows KOH + O_2$ (R8) inhibit sulfation.

It is important to evaluate why the present model strongly overpredicts the degree of sulfation. Reactions in the moist CO/O_2/SO_2 subset of the mechanism are well established and the short-comings of the model are attributed to the potassium scheme. Fig. 6 above compares modeling predictions for the present mechanism with calculations using the older model of Glarborg and Marshall [41]. For this comparison, the thermodynamic properties in the Glarborg and Marshall model were updated to the present values, along with the rate constant for the homogeneous nucleation of K_2SO_4. The major difference between the two models is that the present mechanism includes the additional sulfation pathways involving $KHSO_3$ and $KOSO_3$ proposed by Hindiyarti et al. [42]. The finding that the Glarborg and Marshall model provides a much better agreement with experiment indicates that sulfation through these additional pathways is strongly overpredicted. However, both the thermodynamic properties and rate constants involve significant uncertainties and more work is required to resolve the discrepancy.

4.2. *Effect of KOH and SO_2 on CO oxidation*

While the transformation of KCl with and without addition of SO_2 has been investigated in previous work, data for KOH are scarce. In the following, results are presented for the effect of KOH on CO oxidation and for its interaction with SO_2. However, since gaseous KOH reacts more rapidly than KCl with the quartz surface of the flow reactor to form potassium silicates, the experimental results must be interpreted with caution.

4.2.1. *Effect of KOH on CO oxidation*

Fig. 9 compares results for CO oxidation with and without addition of KOH as a function of temperature. Compared to the reference case, the values of T_i and T_{50} at 0.75 % O_2 for 212 ppm KOH are shifted upward by around 100 K and 150 K, respectively. The inhibition of CO oxidation by KOH under these conditions is actually smaller than that of KCl; we attribute this to the comparatively larger loss of KOH at the reactor wall. For 5 % O_2, presence of KOH shifts the initiation temperature upward by around 50 K in comparison with the reference condition, with the inhibition pronounced at temperatures of 1023–1223 K.

The inhibition of CO oxidation in the presence of KOH is overpredicted for both oxygen levels, most pronounced at 5 % O_2. The discrepancy can be attributed to uncertainties in the experimental conditions, mainly loss of KOH on the reactor surface, or to shortcomings of the chemical kinetic model. As discussed below, there are indications that the surface loss of KOH is strongly underpredicted.

4.2.2. *Effect of SO_2 on CO oxidation in the presence of KOH*

The influence of SO_2 addition on the gas-phase CO/KOH system is illustrated in Fig. 9. Due to the complexity of the experiments with KOH addition, repetitions were conducted for experiments with CO oxidation in the presence of both KOH and SO_2. The results of the repeated experiments were in good agreement with the initial data in the same condition. At 0.75 % O_2 (Fig. 9 (a)), the presence of SO_2 strongly promotes reaction in the CO/KOH system, lowering the initiation temperature from 1150 K to 1050 K. At 5 % O_2 (Fig. 9 (b)), the effect of SO_2 is less pronounced, shifting the conversion temperature for CO about 50 K to lower values. Compared to the results for KCl addition, the impact of SO_2 is more pronounced for KOH, implying that KOH is more readily sulfated.

The experimental results for the CO/KOH/SO_2 system are predicted comparatively well by the model. In agreement with experiment, the model predicts that presence of SO_2 largely cancels the inhibiting effect of KOH on CO oxidation.

4.2.3. *Effect of both NO and SO_2 on CO oxidation in the presence of KOH*

The influence of NO on the CO/KOH system in the presence and absence of SO_2 is demonstrated in Fig. 10. Comparison of the results with those of Fig. 9 shows that addition of NO has only a small impact on the CO/KOH system. However, in the presence of SO_2, NO significantly promotes CO oxidation. The onset of oxidation in the CO-KOH-NO-SO_2 system is shifted approximately 100 K to lower temperature compared to experimental results obtained without SO_2. The concentration of NO is largely constant, with only a small fraction converted to NO_2. The promoting effect of NO on reaction in the CO/SO_2 system has also been reported in the absence of alkali species [30]. The simulations are in satisfactory agreement with the experimental results, both with and without SO_2.

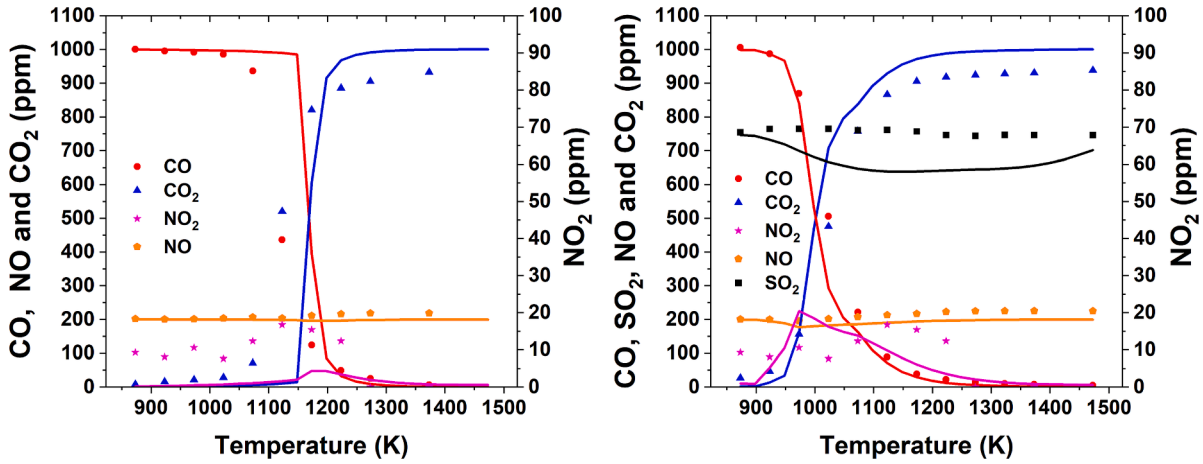

Fig. 10. Comparison of measured and predicted data for outlet gases in the CO/KOH/NO/SO_2/O_2/H_2O system. Inlet condition: 1000 ppm CO, 200 ppm NO, 212 ppm KOH, without SO_2 (left) and with 750 ppm SO_2 (right), 5 % O_2, 3.2 % H_2O; N_2 balance. The residence time is 92/T(K) in the isothermal area at 823–1473 K. Symbols denote experimental data; solid lines denote modeling prediction results.

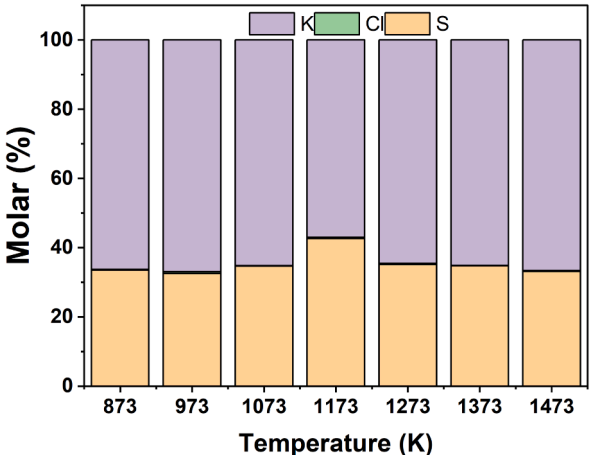

Fig. 11. SEM-EDX data of collected samples in the CO/KOH/SO_2/O_2/H_2O system. Inlet condition: 1000 ppm CO, 212 ppm KOH, 750 ppm SO_2, 5 % O_2, 3.2 % H_2O; N_2 balance (see Fig. 9).

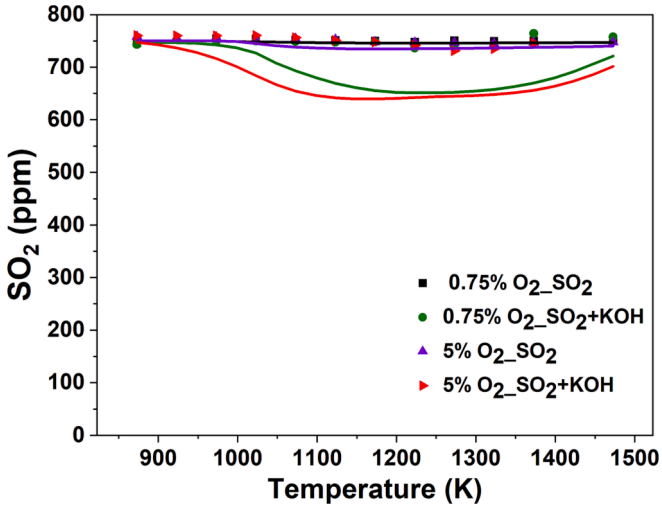

Fig. 12. Comparison of measured and predicted data for SO_2 profiles in the CO/KOH/SO_2/O_2/H_2O system. Inlet condition: 1000 ppm CO, 0 or 212 ppm KOH, 750 ppm SO_2, 0.75 % or 5 % O_2, 3.2 % H_2O; N_2 balance. The residence time is 92/T(K) in the isothermal area at 823–1473 K. Symbols denote experimental data; solid lines denote modeling prediction results.

4.2.4. *Sulfation of KOH by SO_2*

Fig. 11 shows the chemical composition from SEM-EDX analysis of the particles collected in the downstream filter for the CO-KOH-SO_2 system at different temperatures. The composition of the fine particles is composed of K and S in molar proportions consistent with K_2SO_4. The results show that KOH has undergone sulfation in the presence of SO_2 in the entire temperature range. Comparison with the data for KCl shows that the transformation of KOH to the less corrosive K_2SO_4 proceeds more easily than that of KCl in the presence of SO_2 in the CO-O_2-H_2O system. This finding is in good agreement with the results obtained by Mortensen et al. [15] and Weng et al. [35]. The modeling predictions indicate that the KOH is almost fully sulfated in the whole temperature covered, consistent with the experimental results.

Fig. 12 compares the measured and predicted concentrations of SO_2 in the CO-KOH-SO_2 system. Surprisingly, only a small consumption of SO_2 is observed, mostly limited to a temperature window about 1200–1350 K for both oxygen levels. Together with the finding that the filter K was fully sulfated, this is an indication that the KOH is largely captured on the reactor walls as potassium silicates, rather than reacting in the gas-phase. This is consistent with the observation that more SO_2 is consumed by reaction with KCl compared to KOH, even though KOH is more easily sulfated. The loss of KOH is underpredicted significantly by the model, even though it is assumed to be controlled by diffusion to the reactor surface. However, loss of KOH prior to the isothermal zone in the reactor is unaccounted for.

4.2.5. *Reaction flow and sensitivity analyses*

Fig. 7 above shows the reaction paths for transformation of KOH in CO oxidation at 5 % O_2 at the temperature for 50 % conversion. The reaction paths in black are important for both KOH and KCl, while those in blue are specific for KOH. The main pathways are similar for the two potassium salts, taking place mainly through the intermediates $KOSO_3$ and $KHSO_4$. As the SO_3 builds up from the oxidation of SO_2, KOH is converted mainly to $KHSO_4$ by reaction with SO_3,

$$KOH + SO_3 + M \rightleftarrows KHSO_4 + M \quad \text{(R17)}$$

$KHSO_4$ is partly converted directly to K_2SO_4 by reaction with KOH,

$$KHSO_4 + KOH \rightleftarrows K_2SO_4 + H_2O \quad \text{(R25)}$$

Other pathways involve $KOSO_2$ and $KOSO_3$, similar to predictions for KCl.

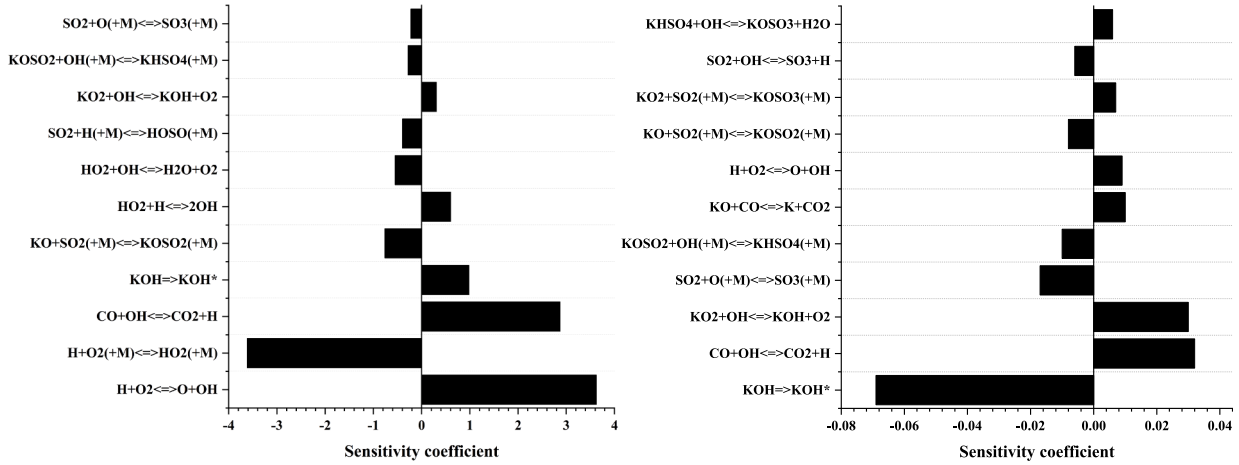

Fig. 13. A-factor sensitivity coefficients for prediction of CO_2 (left) at the 50 % conversion temperature (1035 K) and K_2SO_4 (1173 K) (right) for conditions corresponding to Fig. 10 (right).

Fig. 13 shows the sensitivity coefficients for the predicted CO_2 at 1035 K (left) and K_2SO_4 at 1173 K (right). For the CO_2 formation, the reaction H + O_2 (+M) ⇄ HO_2 (+M) (R16) shows up with a large negative sensitivity coefficient; the reaction is the most important for the inhibition of CO oxidation. The reactions CO + OH ⇄ CO_2 + H (*R*3) and H + O_2 ⇄ O + OH (R1) that generate free radicals in the reaction system promote CO oxidation and exhibit large positive sensitivity coefficients. Considering the K-containing intermediates, the analysis show an inhibiting effect of KO_2 + SO_2 + M ⇄ $KOSO_3$ + M (R16), $KOSO_2$ + OH (+M) ⇄ $KHSO_4$ (+M) (R19), and $KHSO_4$ + OH ⇄ $KOSO_3$ + H_2O (R24) that all consume free radicals (OH/H). On the other hand, the chain-branching reaction KOH + O_2 ⇄ KO_2 + OH (R8b) serves to promote CO conversion.

Fig. 13 (right) shows the sensitivity coefficients for the predicted of K_2SO_4 at 1173 K at the location of the maximum predicted sulfation rate. Contrary to the case for KCl, the reactions CO + OH ⇄ CO_2 + H (*R*3) and H + O_2 ⇄ O + OH (R1) here exhibit positive sensitivity coefficients; the HO_2 radical does not play an important role in sulfation of KOH. The reactions KO_2 + SO_2 (+M) ⇄ $KOSO_3$ (+M) (R16) and $KHSO_4$ + OH ⇄ $KOSO_3$ + H_2O (R24) promote KOH sulfation, while $KOSO_2$ + OH (+M) ⇄ $KHSO_4$ (+M) (R19), KO_2 + OH ⇄ KOH + O_2 (R8) inhibit K_2SO_4 formation. The reactions SO_2 + OH ⇄ SO_3 + H (R5b) and SO_2 + O(+M) ⇄ SO_3 (+M) (R4) exhibit negative sensitivity coefficients even though they act to oxidize SO_2 to SO_3.

5. Conclusions

In the present work, the chemical coupling between moist CO oxidation and transformation of gaseous potassium salts (KCl or KOH) in the presence and absence of SO_2 was investigated under fuel-lean conditions at temperatures of 873–1473 K. Experiments were conducted in a flow reactor, with KCl or KOH aerosols generated by an atomizer. The following conclusions can be made:

- Both KCl and KOH act to inhibit CO oxidation through chain-terminating reactions involving potassium. In the presence of SO_2, the potassium salts are partly sulfated; this reduces the inhibiting effect of K-species since K_2SO_4 does not participate in radical removal. Presence of NO further promotes reaction.
- KCl was only sulfated to a small degree, while KOH reacting in the gas phase was fully sulfated. The interpretation of the experiments was made difficult by depletion of particularly KOH at the quartz reactor walls.
- A chemical kinetic model has been established, with updated thermochemistry. It provides a satisfactory prediction of the CO conversion in the presence of K-S-Cl species, but strongly overpredicts sulfation of KCl. Analysis of the calculations indicates that sulfation pathways in the model involving $KOSO_3$ contribute to the overprediction, but both the thermodynamic properties and rate constants in the model involve significant uncertainties and more work is required to resolve the discrepancy.

CRediT authorship contribution statement

Arphaphon Chanpirak: Conceptualization, Methodology, Writing – original draft. **Hamid Hashemi:** . **Flemming J. Frandsen:** . **Hao Wu:** Supervision, Writing – review & editing. **Peter Glarborg:** Supervision, Writing – review & editing. **Paul Marshall:** Writing – review & editing.

Declaration of Competing Interest

The authors declare that they have no known competing financial interests or personal relationships that could have appeared to influence the work reported in this paper.

Data availability

Data will be made available on request.

Acknowledgments

This work was supported by Ørsted A/S and the Technical University of Denmark. A.C. is grateful for funding from the Thailand Education and Training Abroad Center and Naresuan University, Thailand.

Appendix A. Supplementary data

Supplementary data to this article can be found online at https://doi.org/10.1016/j.fuel.2022.127127.

References

[1] Vassilev SV, Baxter D, Andersen LK, Vassileva CG, Morgan TJ. An overview of the organic and inorganic phase composition of biomass. Fuel 2012;94:1–33.
[2] Knudsen JN, Jensen PA, Dam-Johansen K. Transformation and release to the gas phase of Cl, K, and S during combustion of annual biomass. Energy Fuels 2004;18:1385–99.
[3] Van Lith SC, Alonso-Ramírez V, Jensen PA, Frandsen FJ, Glarborg P. Release to the gas phase of inorganic elements during wood combustion. Part 1: development and evaluation of quantification methods. Energy Fuels 2006;20:964–78.

[4] Johansen JM, Jakobsen JG, Frandsen FJ, Glarborg P. Release of K, Cl, and S during pyrolysis and combustion of high-chlorine biomass. Energy Fuels 2011;25:4961–71.
[5] Jensen PA, Frandsen FJ, Hansen J, Dam-Johansen K, Henriksen N, Ho S. SEM Investigation of Superheater Deposits from Biomass-Fired Boilers. Energy Fuels 2004;12:378–84.
[6] Michelsen HP, Frandsen F, Dam-Johansen K, Hede O. Deposition and high temperature corrosion in a 10 MW straw fired boiler. Fuel Process Technol 1998;54:95–108.
[7] Themelis NJ. Chlorine sources, sinks, and impacts in wte power plants. 18th Annu North Am. Waste-to-Energy Conf NAWTEC 2010;18:77–84.
[8] Ma W, Hoffmann G, Schirmer M, Chen G, Rotter VS. Chlorine characterization and thermal behavior in MSW and RDF. J Hazard Mater 2010;178:489–98.
[9] Aracil I, Font R, Conesa JA. Semivolatile and volatile compounds from the pyrolysis and combustion of polyvinyl chloride. J Anal Appl Pyrol 2005;74:465–78.
[10] Zhou H, Meng A, Long Y, Li Q, Zhang Y. An overview of characteristics of municipal solid waste fuel in China: physical, chemical composition and heating value. Renew Sustain Energy Rev 2014;36:107–22.
[11] Yuan G, Chen D, Yin L, Wang Z, Zhao L, Wang JY. High efficiency chlorine removal from polyvinyl chloride (PVC) pyrolysis with a gas-liquid fluidized bed reactor. Waste Manag 2014;34:1045–50.
[12] Cao W, Lue L, Zhang X. Release of alkali metals during biomass gasification. Arch Ind Biotechnol 2016;1:1–3.
[13] Wei X, Schnell U, Hein KRG. Behaviour of gaseous chlorine and alkali metals during biomass thermal utilisation. Fuel 2005;84:841–8.
[14] Niu Y, Tan H, Hui S. Ash-related issues during biomass combustion: Alkali-induced slagging, silicate melt-induced slagging (ash fusion), agglomeration, corrosion, ash utilization, and related countermeasures. Prog Energy Combust Sci 2016;52:1–61.
[15] Mortensen MR, Hashemi H, Wu H, Glarborg P. Modeling post-flame sulfation of KCl and KOH in bio-dust combustion with full and simplified mechanisms. Fuel 2019;258:116147.
[16] Nielsen HP, Frandsen FJ, Dam-Johansen K, Baxter LL. The implications of chlorine-associated corrosion on the operation of biomass-fired boilers. Prog Energy Combust Sci 2000;26:283–98.
[17] Schofield K. The chemical nature of combustion deposition and corrosion: the case of alkali chlorides. Combust Flame 2012;159(5):1987–96.
[18] Theis M, Skrifvars BJ, Zevenhoven M, Hupa M, Tran H. Fouling tendency of ash resulting from burning mixtures of biofuels. Part 2: deposit chemistry. Fuel 2006;85:1992–2001.
[19] Lith SCV, Frandsen FJ, Montgomery M, Vilhelmsen T, Jensen SA. Lab-scale investigation of deposit-induced chlorine corrosion of superheater materials under simulated biomass-firing conditions. Part 1: exposure at 560 °C. Energy Fuels 2009;23(7):3457–68.
[20] Glarborg P. Hidden interactions-trace species governing combustion and emissions. Proc Combust Inst 2007;31:77–98.
[21] Alzueta MU, Bilbao R, Glarborg P. Inhibition and sensitization of fuel oxidation by SO_2. Combust Flame 2001;127:2234–51.
[22] Abián M, Giménez-López J, Bilbao R, Alzueta MU. Effect of different concentration levels of CO_2 and H_2O on the oxidation of CO: Experiments and modeling. Proc Combust Inst 2011;33(1):317–23.
[23] Hindiyarti L, Frandsen F, Livbjerg H, Glarborg P. Influence of potassium chloride on moist CO oxidation under reducing conditions: experimental and kinetic modeling study. Fuel 2006;85:978–88.
[24] Chanpirak A, Wu H, Glarborg P. An experimental and chemical kinetic modeling study of the role of potassium in the moist oxidation of CO. Fuel 2023;335:127035.
[25] Marinkovic J, Thunman H, Knutsson P, Seemann M. Characteristics of olivine as a bed material in an indirect biomass gasifier. Chem Eng J 2015;279:555–66.
[26] Bulewicz EM, Janicka E, Kandefer S. Halogen inhibition of CO oxidation during the combustion of coal in fluidized bed. Proc 10th Int Conf Fluid Bed Combust FBC–Technology Today 1989:163–8.
[27] Thunman H, Seemann M, Berdugo Vilches T, Maric J, Pallares D, Ström H, et al. Advanced biofuel production via gasification – lessons learned from 200 man-years of research activity with Chalmers' research gasifier and the GoBiGas demonstration plant. Energy Sci Eng 2018;6:6–34.
[28] Berdugo Vilches T, Weng W, Glarborg P, Li Z, Thunman H, Seemann M. Shedding light on the governing mechanisms for insufficient CO and H_2 burnout in the presence of potassium, chlorine and sulfur. Fuel 2020;273:117762.
[29] Ekvall T, Andersson K. Experimentally observed influences of KCl and SO_2 on CO oxidation in an 80 kW oxy-propane flame. 34th Annu. Int. Pittsburgh Coal Conf Coal - Energy, Environ Sustain Dev 2017.
[30] Glarborg P, Kubel D, Dam-Johansen K, Chiang HM, Bozzelli JW. Impact of SO_2 and NO on CO oxidation under post-flame conditions. Int J Chem Kinet 1996;28:773–90.
[31] Allgurén T, Andersson K. Influence of KCl and SO_2 on NO Formation in C_3H_8 Flames. Energy Fuels 2017;31:11413–23.
[32] Ekvall T, Andersson K, Leffler T, Berg M. K-Cl-S chemistry in air and oxy-combustion atmospheres. Proc Combust Inst 2017;36:4011–8.
[33] Weng W, Zhang Y, Wu H, Glarborg P, Li Z. Optical measurements of KOH, KCl and K for quantitative K-Cl chemistry in thermochemical conversion processes. Fuel 2020;271:117643.
[34] Weng W, Li Z, Wu H, Aldén M, Glarborg P. Quantitative K-Cl-S chemistry in thermochemical conversion processes using in situ optical diagnostics. Proc Combust Inst 2021;38:5219–27.
[35] Weng W, Chen S, Wu H, Glarborg P, Li Z. Optical investigation of gas-phase KCl/KOH sulfation in post flame conditions. Fuel 2018;224:461–8.
[36] Hashemi H, Christensen JM, Gersen S, Levinsky H, Klippenstein SJ, Glarborg P. High-pressure oxidation of methane. Combust Flame 2016;172:349–64.
[37] Jensen JR, Nielsen LB, Schultz-Møler C, Wedel S, Livbjerg H. The nucleation of aerosols in flue gases with a high content of alkali - a laboratory study. Aerosol Sci Technol 2000;33:490–509.
[38] Eerikäinen H, Watanabe W, Kauppinen EI, Ahonen PP. Aerosol flow reactor method for synthesis of drug nanoparticles. Eur J Pharm Biopharm 2003;55:357–60.
[39] Andersson V, Soleimanisalim AH, Kong X, Hildor F, Leion H, Mattisson T, et al. Alkali-wall interactions in a laboratory-scale reactor for chemical looping combustion studies. Fuel Process Technol 2021;217:106828.
[40] MANUAL TSI Instruction. Model 3075/3076 Constant Output Atomizer; 2009.
[41] Glarborg P, Marshall P. Mechanism and modeling of the formation of gaseous alkali sulfates. Combust Flame 2005;141:22–39.
[42] Hindiyarti L, Frandsen F, Livbjerg H, Glarborg P, Marshall P. An exploratory study of alkali sulfate aerosol formation during biomass combustion. Fuel 2008;87:1591–600.
[43] Li B, Sun Z, Li Z, Aldén M, Jakobsen JG, Hansen S, et al. Post-flame gas-phase sulfation of potassium chloride. Combust Flame 2013;160:959–69.
[44] Pelucchi M, Frassoldati A, Faravelli T, Ruscic B, Glarborg P. High-temperature chemistry of HCl and Cl_2. Combust Flame 2015;162:2693–704.
[45] Song Y, Hashemi H, Christensen JM, Zou C, Haynes BS, Marshall P, et al. An Exploratory Flow Reactor Study of H_2S Oxidation at 30–100 Bar. Int J Chem Kinet 2017;49:37–52.
[46] Iisa K, Lu Y, Salmenoja K. Sulfation of potassium chloride at combustion conditions. Energy Fuels 1999;13:1184–90.
[47] Curtiss LA, Redfern PC, Raghavachari K. Gaussian-4 theory. J Chem Phys 2007;126(8):084108.
[48] Giménez-López J, Martínez M, Millera A, Bilbao R, Alzueta MU. SO_2 effects on CO oxidation in a CO_2 atmosphere, characteristic of oxy-fuel conditions. Combust Flame 2011;158(1):48–56.
[49] Sengeløv LW, Hansen TB, Bartolomé C, Wu H, Pedersen KH, Frandsen FJ, et al. Sulfation of condensed potassium chloride by SO_2. Energy Fuels 2013;27:3283–9.